Supporting information: Optical Forging of Graphene into Three-Dimensional Shapes

*Andreas Johansson[1,2]†, Pasi Myllyperkiö[1]†, Pekka Koskinen[2], Jukka Aumanen[1], Juha Koivistoinen[1], Hung-Chieh Tsai[3], Chia-Hao Chen[4], Lo-Yueh Chang[4], Vesa-Matti Hiltunen[2], Jyrki J. Manninen[2], Wei Yen Woon[3], Mika Pettersson[1]**

[1]Nanoscience Center, Department of Chemistry, P.O. Box 35, FI-40014, University of Jyväskylä, Finland.

[2]Nanoscience Center, Department of Physics, P.O. Box 35, FI-40014, University of Jyväskylä, Finland.

[3]Department of Physics, National Central University, Jungli, 32054, Taiwan, Republic of China.

[4]National Synchrotron Radiation Research Center, Hsinchu, 30076, Taiwan, Republic of China.

†These authors contributed equally to this work.

*Corresponding author. E-mail: mika.j.pettersson@jyu.fi

Additional Materials and Methods

Samples

Silicon chips (10 mm by 10 mm in size with a top-layer of 300 nm SiO_2) with a monolayer of chemical vapor deposition grown graphene on top were purchased from Graphenea Inc. A reference grid was patterned on the top surface, using electron beam lithography in PMMA. The patterned grid was made of 1 μm wide lines, defining a 10 by 10 matrix of 200 μm by 200 μm squares. Oxygen reactive ion etching was used to remove graphene from the bottom of the pattern, after which it was metallized with 2 nm Ti as adhesion layer and 30 nm Au on top. The chips were covered with an additional PMMA layer as protection, and then diced to our preferred size of 5 mm by 5 mm before finalizing the patterning with a lift-off procedure. The resulting reference grid allowed positioning of irradiated patterns at known locations so that they could be found during characterization measurements.

Direct laser writing

Direct laser writing of the patterns was performed with a setup consisting of an amplified femtosecond laser (Pharos-10, 600 kHz, Light Conversion Ltd.), two non-collinear optical parametric amplifiers (NOPA, Orpheus-N, Light Conversion Ltd.) and a home-built optical microscope with nano-positioning system (Nanomax 300, Thorlabs Inc.). The microscope was equipped with a camera, allowing precise alignment and visual inspection of the sample.

Laser beams were focused to the sample by a microscope objective (Nikon LU Plan ELWD 100x/0.80). The sample was installed to a closed chamber that was purged with argon or nitrogen to prevent oxidation of the graphene during the writing process.

Two different femtosecond laser configurations were used for the writing experiments, short 30-40 fs and longer 250 fs laser pulses. The short pulses were taken from the non-collinear optical parametric amplifier (NOPA, Orpheus-N, Light Conversion Ltd.) and were centered at 560 nm. Pulse energies for the writing were 5 - 25 pJ/pulse. The longer pulses centered at 515 nm were made using the second harmonic generation from the fundamental of the laser and the energy was ~40 pJ/pulse. The writing speed was varied for different structures from 0.1 s to 10 s per spot.

Raman spectroscopy

Raman measurements were carried out with a home-built Raman setup in a backscattering geometry using 532 nm excitation wavelength produced with continuous wave single frequency laser (Alphalas, Monolas-532-100-SM). The beam was focused on a sample and the signal was collected with a 100x microscope objective (Nikon L Plan SLWD 100x with 0.70 N.A.). The scattered light was dispersed in a 0.5 m imaging spectrograph (Acton, SpectraPro 2500i) using 600 g/mm grating (with resolution: ~ 5 - 7 cm^{-1}). The signal was detected with EMCCD camera (Andor Newton EM DU971N-BV) using 60 μm slit width. A beam splitter was placed between the objective and the spectrometer in order to observe the exact measurement point visually. The Rayleigh scattering was attenuated with an edge filter (Semrock). The approximate sample positioning was done with XYZ-piezoscanner (Attocube, ANPxyz101) with smallest step of 50

nm in each direction. A laser power of ~1 mW was utilized and measurement time per accumulation was 5 s. Mapping was conducted using 300 nm steps between measurement points and the total map consisted of 50 x 50 points.

Atomic Force Microscopy

All imaging and characterization was made on a Bruker Dimension Icon atomic force microscope, using Peak Force Tapping mode. ScanAsyst Air probes from Bruker were used during imaging with the peak force limited to 2 nN. Nanoindentation was made with RTESPA-300 probes from Bruker. The cantilever spring constant was determined to be 50.9 N/m, using the Sader method.[1] With a nominal radius of 8 nm, the RTESPA-300 probe tip was just before nanoindentation measurements characterized to have a radius of 31.5 nm. The AFM images in Figure 4 have been smoothed with a Gaussian low-pass filter to suppress noise and visually enhance the patterned 3D structures.

XPS

XPS (X-ray photoelectron spectroscopy) measurement was conducted at National Synchrotron Radiation Research Center, Taiwan (SPEM end station of beamline 09A1). The soft X-ray beam (photon energy 620 eV) was focused with Fresnel zone-plate optics to achieve spatial resolution of 100 nm. The photon energy was routinely calibrated with the core-level line of Au at binding energy 84 eV. The overall energy resolution was better than 100 meV, and the experiments were conducted at room temperature.

Simulations

The elastic modeling of graphene used thin sheet elasticity theory, known to describe deformed graphene over several length scales.[2,3] The in-plane elastic modulus was $k_s = 21$ eV/Å^2, the Poisson ratio $\upsilon = 0.2$, and the bending modulus $k_b = 1.0$ eV.[4,5] The strain tensor $e_{\alpha\beta}(\mathbf{r})$ was modified into $e'_{\alpha\beta}(\mathbf{r}) = e_{\alpha\beta}(\mathbf{r}) - \delta e_{\alpha\beta}(\mathbf{r})$ in order to account for the expansion field $\varepsilon(\mathbf{r})$. To simulate the $2x2$ μm^2 square patterns, we fixed $5x5$ μm^2 sheets at the edges, discretized them on a $200x200$ rectangular grid and optimized to stresses below 10^{-7} eV/Å^2 under the given expansion field using the FIRE method.[6] The flimsiness of sheets required multiple initial guesses to ascertain the topography of the global energy minimum. The substrate was treated as a hard surface, which was justified, because a lower threshold for ε_0, below which the graphene would have preferred to stay flat on the substrate, was not observed in the experiment. The strains in the pyramid levels were calculated from the experimental (cumulative) irradiation times 0.5 s, 1.0 s, 2.0 s, and 3.5 s by using a 3.9×10^{-5} s^{-1} strain rate. Eq. (1) was derived by first noticing that the length expansion across any line profile is $\Delta L = \int \varepsilon(\mathbf{r}) ds$, which for a square pattern of length L_0 becomes $\Delta L_\varepsilon = \varepsilon_0 (L_0 + FWHM \times \sqrt{\pi / \log 16})$. Structure of height h requires an expansion $\Delta L_h = \pi^2 h^2 / 8w$, assuming an edge height profile $h \sin^2(x\pi / 2w)$, where w is the edge width $(h \ll w)$ and x is the distance along the substrate $(0 \le x \le w)$; Eq. (1) follows by setting $\Delta L_\varepsilon = \Delta L_h$.

The atomistic simulations of Stone-Wales (SW) defects were done using the LAMMPS package with the REBO interatomic potential.[7,8] SW defects were created in periodic simulation cells of rectangular shape and varying aspect ratio; the SW defect density was the inverse of the

cell area. Structures were optimized to maximum force criterion 0.5 meV/Å under a planar constraint and the mean expansion was calculated from the stress tensor.

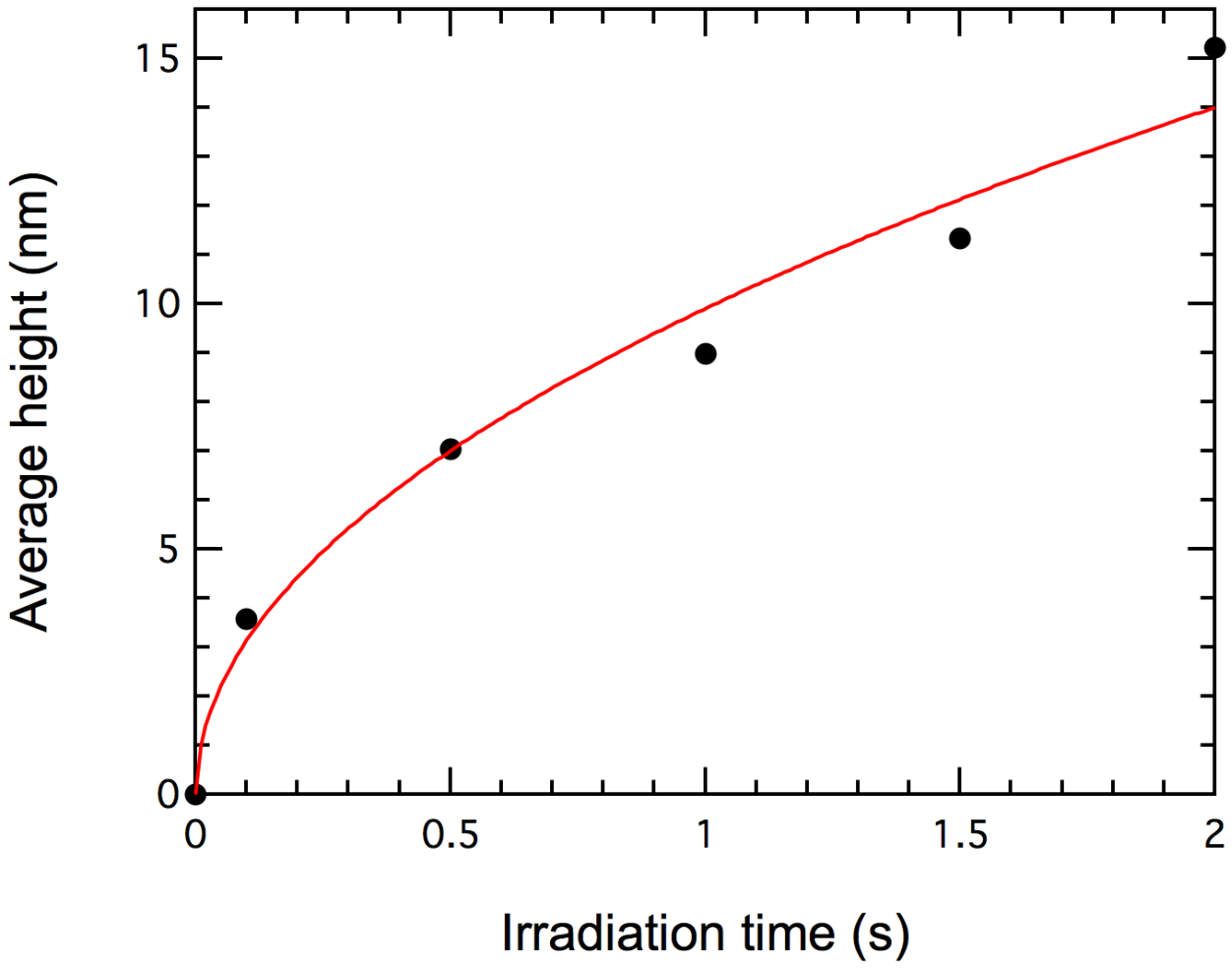

Figure S1. Height of elevated structures as a function of irradiation time per spot. The height data is extracted from the AFM data set in Figure 1a. The red curve shows a fit to square root dependence on the irradiation time.

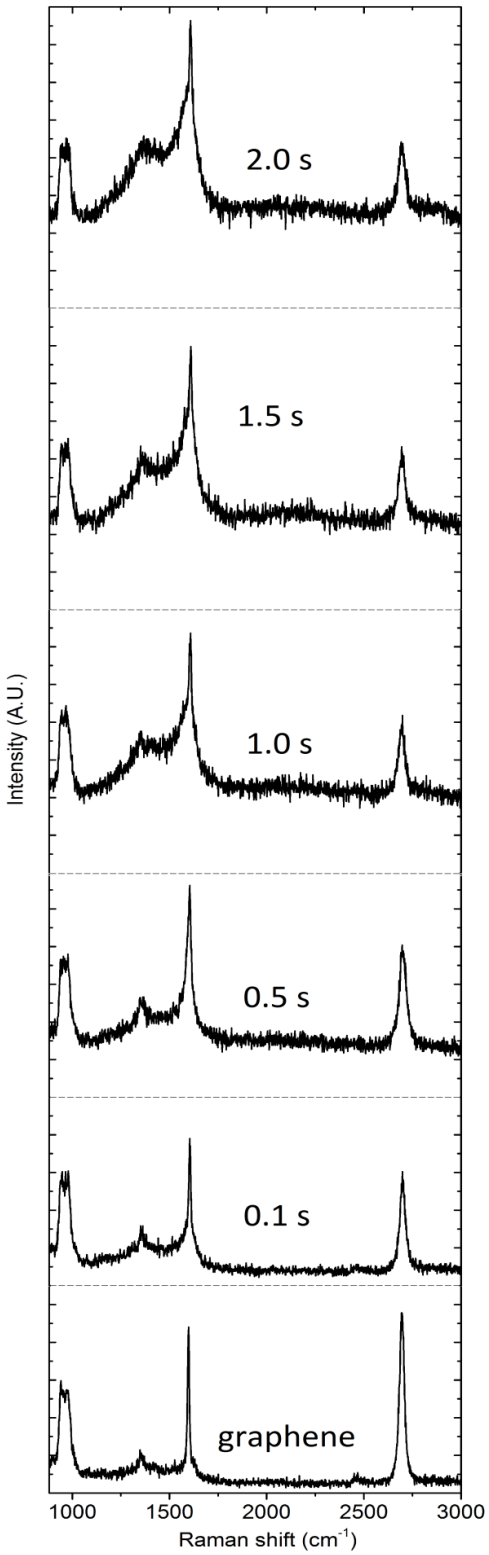

Figure S2. Raman spectra from the sample in Fig. 1. The labels show the irradiation time per spot. The dashed line indicates the 0-level of the signal.

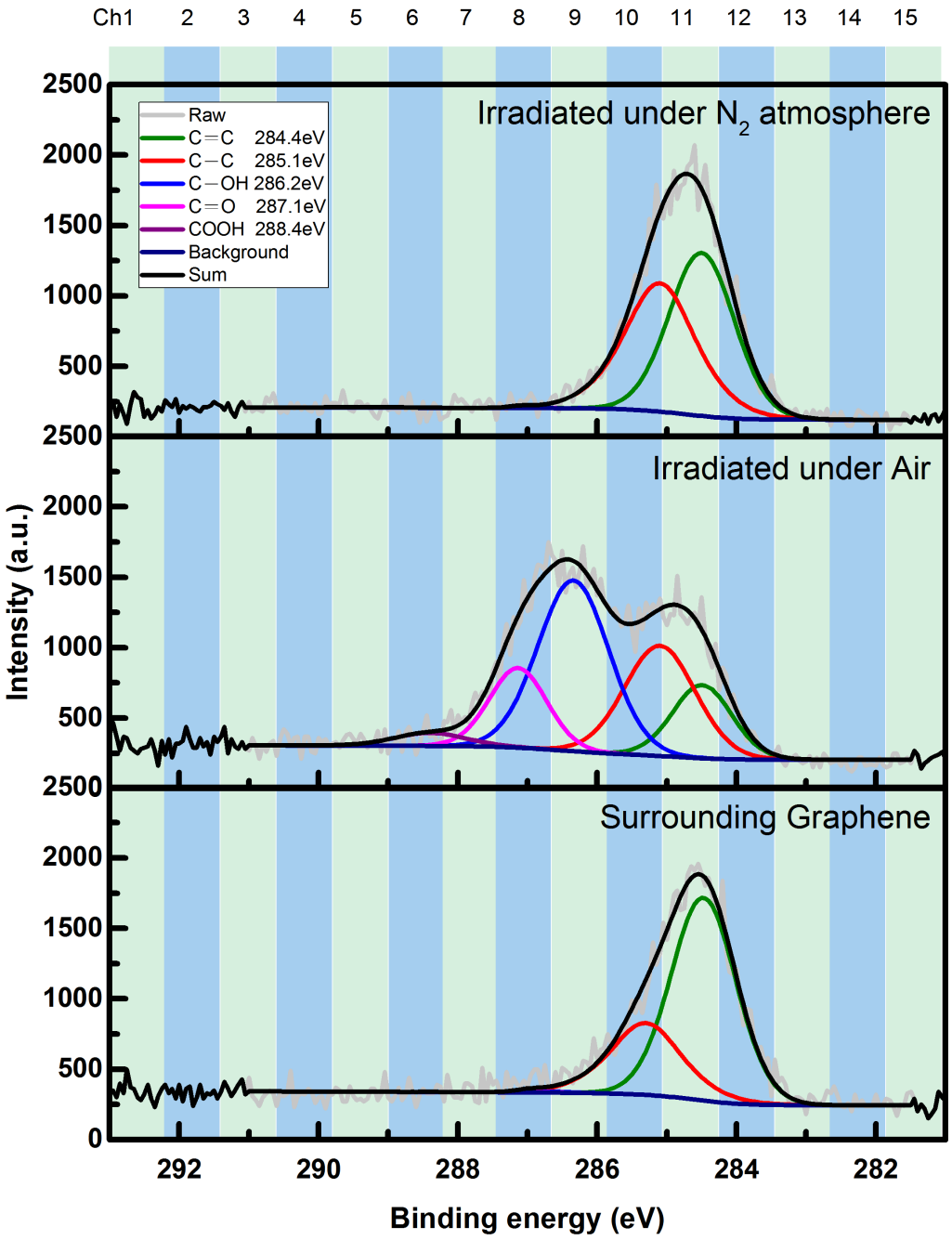

Figure S3. Comparison of XPS data for non-irradiated graphene (bottom), graphene irradiated under N_2 atmosphere (top), and graphene irradiated under air atmosphere (middle). All the areas were located on the same sample.

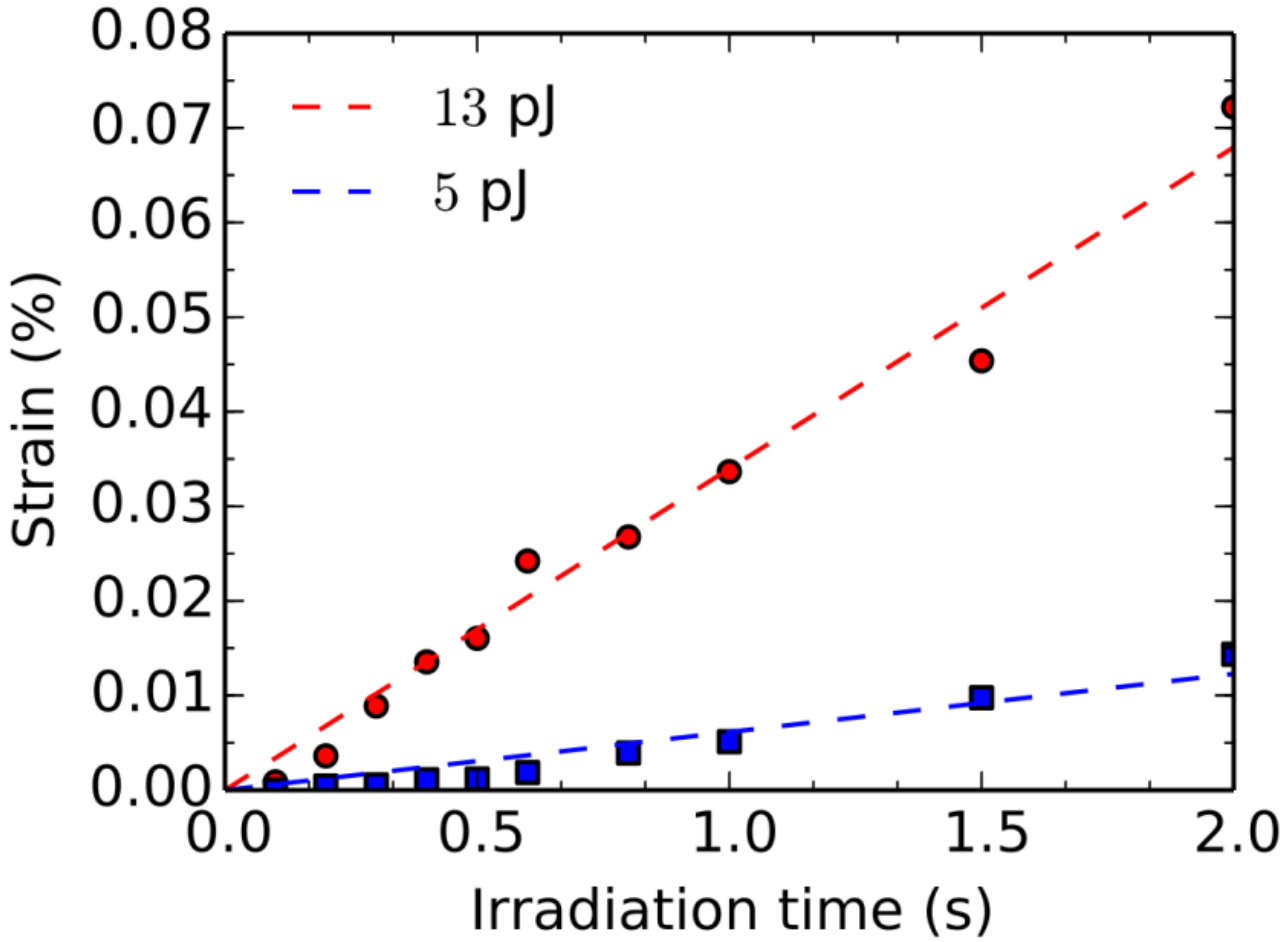

Figure S4. Strain as a function of irradiation time. The curves were obtained by inverting Eq. (1) for $\varepsilon_0(t) = \varepsilon_0(h(t))$ and using experimental data for square plateaus up to 50 nm in height. The linear fits for the growth rates are 3.5×10^{-4} (13 pJ pulses) and 6.1×10^{-5} 1/s (5 pJ pulses).

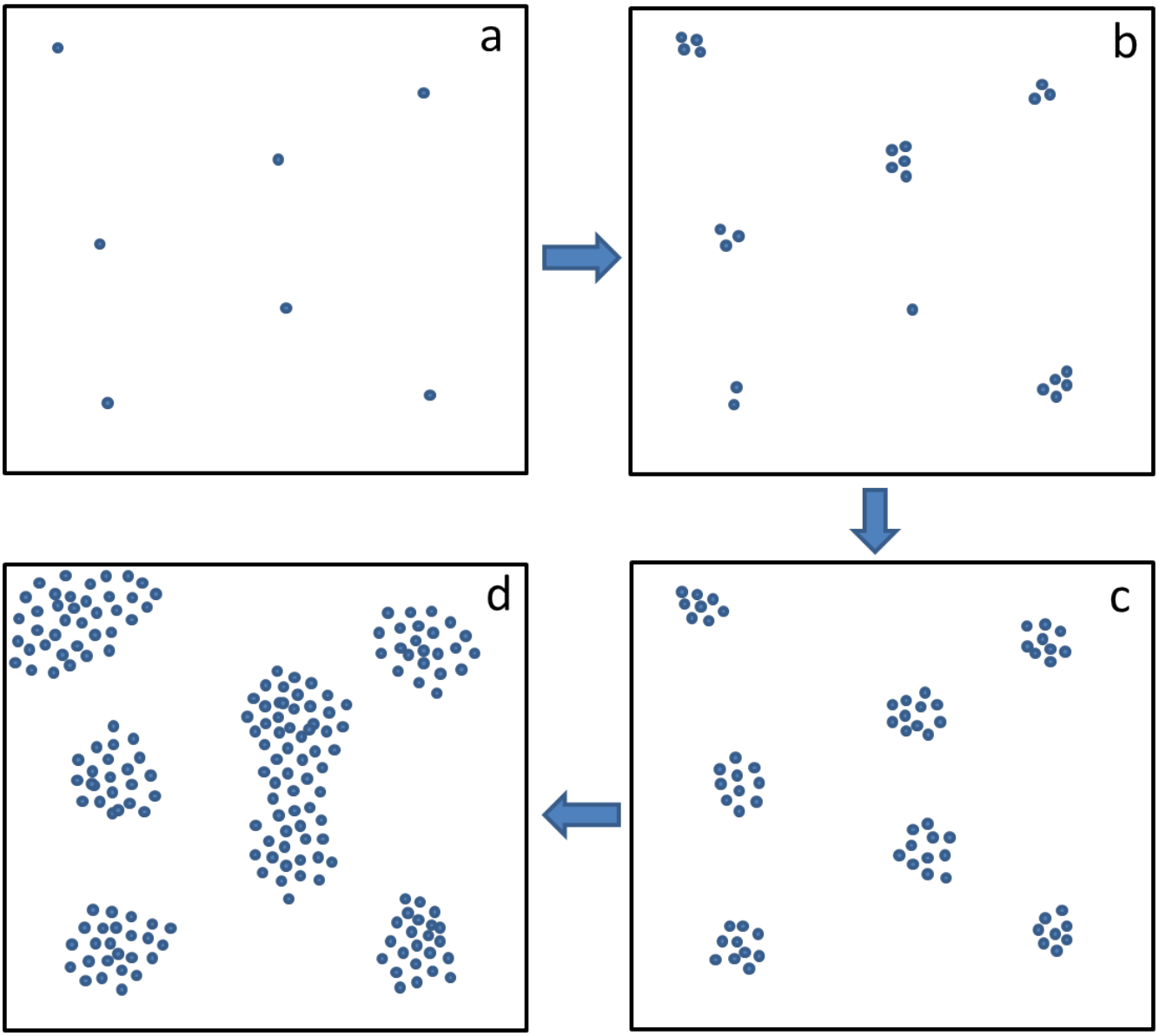

Figure S5. Cartoon showing the proposed mechanism of defect formation in graphene upon irradiation. a) Initially point defects (blue dots) are formed in graphene. b) New defects form preferentially close to existing defects. c) More defects lead to regions that are disordered. d) The area of disordered regions grows as new defects are formed, eventually leading to coalescence of the defected regions.

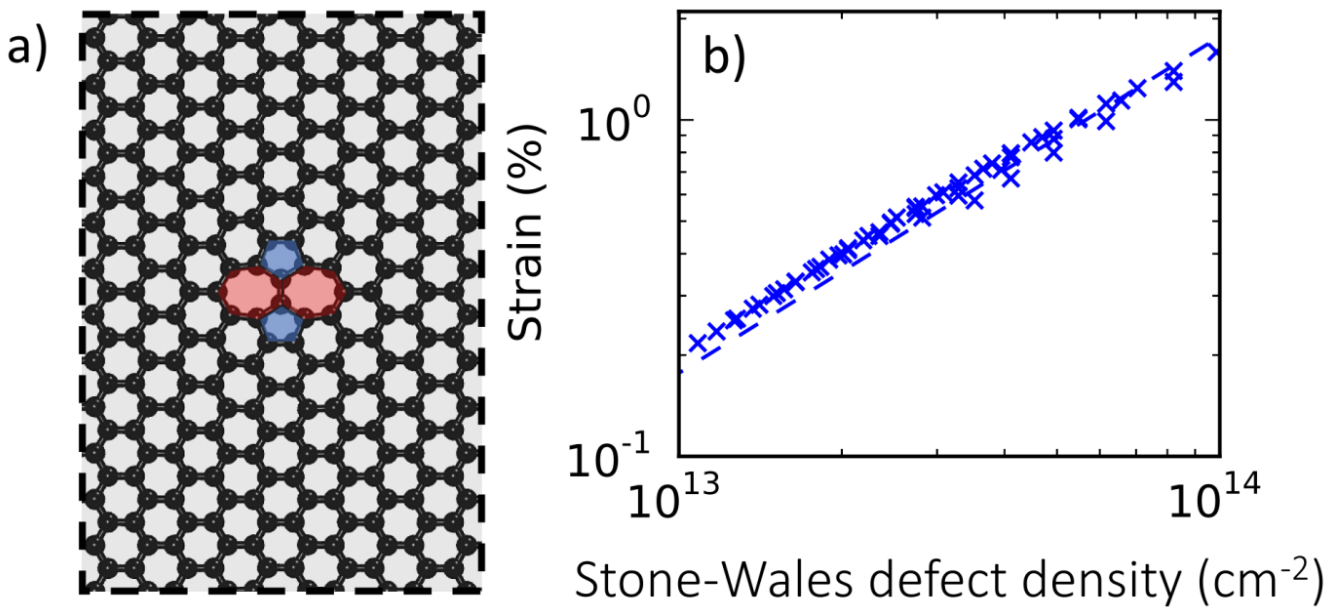

Figure S6. Lattice expansion with Stone-Wales defects. a) Stone-Wales defect in a rectangular unit cell, optimized with REBO potential under planar constraint. b) Biaxial strain in the unit cell as a function of defect density (inverse of unit cell area); defect density was changed by varying cell size and aspect ratio.

REFERENCES

(1) Sader, J. E.; Chon, J. W. M.; Mulvaney, P. *Rev. Sci. Instrum.* **1999**, *70* (10), 3967–3969.

(2) Landau, L. D.; Lifshitz, E. M. *Theory of Elasticity*, 3rd ed.; Pergamon: New York, 1986.

(3) Neto, A. C.; Guinea, F.; Peres, N.; Novoselov, K. S.; Geim, A. K. *Rev. Mod. Phys.* **2009**, *81* (1), 109–162.

(4) Do Carmo, M. P. *Differential Geometry of Curves and Surfaces*; Prentice-Hall: New Jersey, 1976.

(5) Koskinen, P.; Kit, O. O. *Phys Rev B* **2010**, *82* (23), 235420.

(6) Bitzek, E.; Koskinen, P.; Gähler, F.; Moseler, M.; Gumbsch, P. *Phys Rev Lett* **2006**, *97* (17), 170201.

(7) Plimpton, S. *J. Comp. Phys.* **1995**, *117* (1), 1–19.

(8) Brenner, D. W.; Shenderova, O. A.; Harrison, J. A.; Stuart, S. J.; Ni, B.; Sinnott, S. B. *J. Phys. Cond. Mat.* **2002**, *14* (4), 783–802.